Desalination and Water Treatment
www.deswater.com
doi:10.5004/dwt.2019.23676

147 (2019) 343–361
April

Grafting of polyamidoamine dendrimer on polyacrylonitrile nanofiber surface: synthesis and optimization of anionic dye removal process by response surface methodology method

Arash Almasian[a,*], Mohammad Ebrahim Olya[a], Niyaz Mohammad Mahmoodi[a], Ehsan Zarinabadi[b]

[a]*Department of Environmental Research, Institute for Color Science and Technology, Tehran, Iran, emails: arashalmasi@yahoo.com (A. Almasian), olya-me@icrc.ac.ir (M.E. Olya), mahmoodi@icrc.ac.ir (N.M. Mahmoodi)*
[b]*Department of Textile, Yazd Branch, Islamic Azad University, Yazd, Iran, email: E.zarinabadi@gmail.com*

Received 1 December 2017; Accepted 22 December 2018

ABSTRACT

In this paper, the surface of polyacrylonitrile (PAN) nanofiber was modified by polyamidoamine (PAMAM) and its dye removal ability was investigated. In this regard, PAN polymer was functionalized by diethylenetriamine (DETA), and the PAMAM dendrimer molecule was grafted to the surface of functionalized nanofiber by glutaraldehyde. The characterization of nanofibers showed that PAMAM molecules were attached to DETA through the formation of amine groups. Scanning electron microscope images of functionalized and surface grafted PAN nanofiber showed a rough surface and deposition of a dense layer on the nanofiber surface, respectively. Also, the surface average roughness of nanofibers increased from 42.4–46.4 nm and 68.6–81.9 nm for PAN-DETA and PAMAM grafted PAN-DETA compared to untreated PAN nanofiber, respectively. The result of the adsorption study showed that the adsorption process followed Langmuir isotherm and pseudo-second-order kinetic models. The dye removal conditions were optimized by the response surface methodology (RSM) model. The RSM result indicated that pH variable is more effective in dye adsorption. It was observed that the amounts of the dye adsorbed onto the prepared nanofiber were influenced by the initial pH, contact time, initial concentrations of the dye solutions, and ionic strength. The prepared nanofibers showed good regeneration ability and high adsorption capacities even after ten adsorption/desorption cycles.

Keywords: Polyacrylonitrile (PAN); Electrospinning; Polyamidoamine; Surface modification; Direct Red 80; Direct Red 23; Adsorption isotherm; Adsorption kinetic

1. Introduction

The presence of numerous dyes in wastewater from different industries has provoked serious environmental concerns all over the world [1,2]. The discharge of these pollutants into natural waterways environmentally unacceptable due to toxic carcinogenic nature of dyes [3]. Thus, removal of dyes from industrial effluents before discharging is necessary. In this regard, several treatment methods have been investigated extensively for dye removal such as biological, chemical, and physical processes [4–9]. The adsorption process is considered to be superior to other techniques because of low cost, the simplicity of design, producing a high-quality effluent, handling of large flow rates, availability, and ability to treat dyes. The affinity of solutes to an adsorbent may be predominantly due to: (1) electrical attraction of the solute to the adsorbent (exchange adsorption): (2) van der Waals attraction (physical or ideal

* Corresponding author.

adsorption): or, (3) chemical reaction (chemisorption or chemical adsorption). Among them, the chemical reaction has been identified by chemists as the major adsorption mechanism for adsorption of dyes [10,11]. At this point, preparation of surface modified adsorbents with functional groups such as amine and carboxyl is interested as a simple and versatile route [12–14]. Many adsorbents are available in different scales for wastewater applications [15–18]. Nanofibers are nanoscopic materials that are widely used in water treatment process due to their small interfibrous pore size, the enormous surface area per unit volume, high porosity, and high gas permeability.

A wide variety of microscale adsorbents have some disadvantages, such as a poor separation ability and low adsorption capacity for dyes. In this regard, researchers have focused on the utilization of nanoscale adsorbents such as nanofibers because of their superior advantages for wastewater applications. Recently, electrospun polyacrylonitrile (PAN) mats are introduced as inexpensive commercial products with desirable chemical and thermal properties [19]. The presence of a nitrile group in the polymer structure enables the polymer to react with primary amine-containing compounds [20].

Dendrimers are known as a family of highly branched three-dimensional polymers containing functional end groups. Polyamidoamine (PAMAM) with high-density of amine terminal group is the most-studied dendrimer in catalysis, molecular recognition, medical science, and purification of water due to its low cost of production via a simple one-pot reaction, its binding capacity for various pollutants and its reusability[21–24]. Many attempts are performed on surface modification of PAN nanofibers using ethylenediamine and diethylenetriamine (DETA) compounds for adsorption of heavy metals [25–27]. PAN-DETA composite nanofibers with the adsorption capacity of 1,250 mg g^{-1} for anionic dyes were prepared previously. Previously, our team investigated the dye removal ability of PAN/PAMAM composite nanofibers [20]. The composite nanofibers showed the adsorption capacity of 2,000 mg g^{-1} toward anionic dyes. Also, PAMAM dendrimer was used for enhancing the filtration efficiency of polytetrafluoroethylene membrane [28]. Hyperbranched poly(amidoamine) was applied for the preparation of functional polysulfone membrane with heavy metal ion binding capability [29]. Also, PAMAM used for functionalizing and increasing the adsorption capacity of inorganic adsorbent [30]. It can be stated that the PAMAM was turned to a conventional compound used in different applications such as wastewater treatment. However, a literature review showed that PAMAM dendrimer was not used for surface modification of PAN nanofibers. Since, the presence of active sites on the surface of adsorbent resulted in higher adsorption capacity values, in this study, PAMAM grafted PAN/DETA nanofiber was prepared by electrospinning technique and the ability of as-prepared nanofibers to remove anionic dyes was investigated. Furthermore, the influence of several parameters such as adsorbent amount, dye concentration, ionic strength, and pH on the adsorption capacity was evaluated. Moreover, many papers deled on adsorption of dyes in a standard method [30–34]. In this study, response surface methodology (RSM) was used for designing experiments and lowers the number of experiments.

2. Experimental section

2.1. Materials

PAN copolymer (93.7% acrylonitrile and 6.3% vinyl acetate with Mw = 100.000 g mol^{-1}) was purchased from Isfahan Polyacryl Inc. (Iran). *N*,*N*–dimethylformamide (DMF), glutaraldehyde (50% in water) and (DETA; ~99% purity) were used as received from Merck. PAMAM dendrimer, Generation a solution of 3, 20 wt.% in methyl alcohol was used as received from Aldrich. direct red 80 (DR80) and direct red 23 (DR23) supplied by AlvanSabet Co. (Iran). The chemical structure of dyes is shown in Fig. 1.

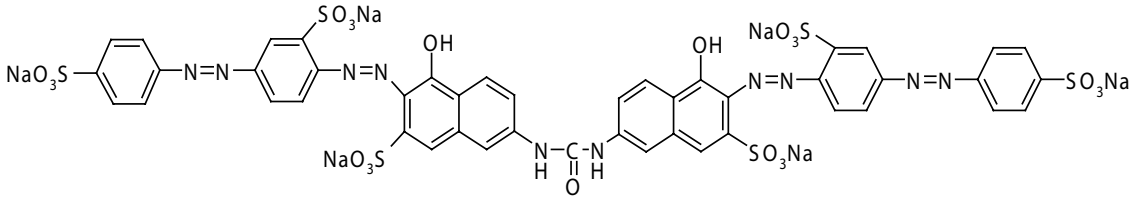

Direct Red 80

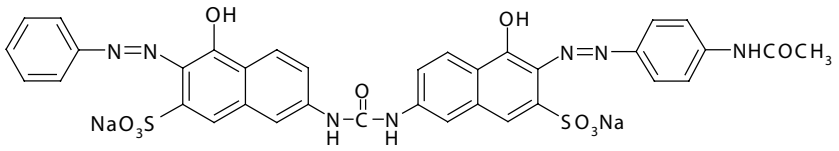

Direct Red 23

Fig. 1. The chemical structure of dyes.

2.2. Preparation of PAN-DETA nanofiber

We accordingly synthesized several samples with a similar composition in our former studies. Hereby we used an optimized nanoweb from those reported for dye removal studies [35]. briefly, electrospinning solution was prepared by dissolving 10 w/w% PAN in DMF under mechanical stirring for 12 h at room temperature in order to obtain a homogeneous solution. The mixture of PAN-DETA solution was then prepared by adding a 20 w/w% DETA into 10 w/w% PAN solution. The mixture was stirred at 95°C for 4 h. The as-prepared solution was then electrospun under a fixed electric field of 17 kV, using a Gamma High Voltage Research RR60 power supply, onto aluminum (Al) sheet as the collector. The distance from the tip to the collector was 15 cm and the feeding rate of the polymer solution was 1.2 mL h^{-1}. All nanofibers were immersed in a distilled water batch (250 mL) containing 1 g potassium carbonate at 80°C for 2 h. Finally, nanofibers were washed by distilled water and dried in an oven (60°C, 3 h).

2.3. Surface grafting of PAMAM onto PAN-DETA nanofiber

The aminated PAN nanofiber was immersed in a batch containing 50 mL of water and 5 mL of glutaraldehyde for 24 h. The nanofiber was then immersed in a batch containing 30 mL of methanol and 2 mL of PAMAM. After evaporation of the solvent, the nanofiber was placed in an oven at 105°C for 2 h and then washed with distilled water to remove unreacted PAMAM molecules from surface modified PAN.

2.4. Characterization

The IR spectra of different nanofibers were examined by attenuated total reflection Fourier transform infrared (ATR-FTIR) spectrometer, (ThermoNicolet NEXUS 870 FTIR from Nicolet Instrument Corp., USA). The surface morphology and topography of all electrospun nanofibers were investigated using a Scanning electron microscope (SEM, LEO1455VP, England) and atomic force microscope (AFM, DualScope C-26, Denmark), respectively. Measurement of the surface area of the nanofibers was carried out using standard Brunauer–Emmett–Teller (BET) analyzer (Micromeritics Gemini III 2375, U.S.A.). Pore size distributions were calculated using the Barret-Joyner-Halenda (BJH) model based on the nitrogen desorption isotherm by a porosimeter (autoporeIV9500, micromeritics Co., U.S.A.).

The isoelectric point (IEP) of synthesized nanofibers was determined by the reported method [30]. The IEP of PAN-DETA and PAMAM grafted nanofibers was 6 and 5.1, respectively.

2.5. Adsorption studies

The adsorption measurements were conducted by mixing the PAMAM grafted PAN-DETA nanofiber in a batch containing 200 mL of a dye solution (40 mg L^{-1}) at pH of 3.5. The pH of each solution was adjusted to the desired value using HCl or NaOH solution. The effect of adsorbent dosage on dye removal was investigated by contacting 200 mL of dye solution (40 mg L^{-1}) at room temperature and pH = 3.5 for 60 min. Different amounts of adsorbent (0.001–0.008 g) were applied. The effect of initial dye concentration on the dye removal was studied by adding 0.004 g of adsorbent to different dye concentrations (40, 60, 80, and 100 mg L^{-1}) at pH = 3.5, and 200 mL of the dye solution. The effect of pH on dye removal was conducted by adding 0.004 g adsorbent, and 200 mL of dye solution (40 mg L^{-1}) at different pH values (2.1, 2.5, 3, 3.5, 6.5, and 9.1). Also, the effect of ionic strength (salts) on dye removal was investigated by the addition of 1 mmol L^{-1} Na_2SO_4 and $CaCl_2$ to the dye solutions and also varying the salt concentrations (1, 2 and 3 mmol L^{-1}).

The amounts of dye removal (%) from solutions were determined as a function of time according to the following equation:

$$\text{Dye removal\%} = \frac{A_0 - A}{A_0} \times 100 \quad (1)$$

where A_0 and A are dye concentration at t = 0 and t, respectively.

In order to study the regeneration and reusability, the adsorbent was immersed in 100 mL of 0.01 M NaOH for 60 min after the completion of the adsorption process. Then it was washed thoroughly with pure water to neutrality and the adsorption was repeated again. The adsorption/desorption process was repeated for ten cycles and the adsorption efficiency and adsorption capacity were investigated.

2.6. Experimental design and optimization

In this study, RSM was used for the experimental design and optimization (Tables 1 and 2). Generally, RSM is a

Table 1
Designing of experience for response of adsorption

Run	PH	Time	Density	DR23	DR80
1	9.175716	16.148402	87.838107	12.97	13.77
2	3.824284	48.851598	87.838107	41	46
3	6.5	32.5	70	42	52
4	6.5	5	70	30	40
5	6.5	32.5	70	50	60
6	2	32.5	70	24	33
7	9.175716	48.851598	87.838107	14.1	15.5
8	6.5	32.5	70	40	53
9	3.824284	16.148402	52.161893	66.5	68.3
10	9.175716	16.148402	52.161893	15.94	17.54
11	3.824284	16.148402	87.838107	36.4	42.2
12	6.5	32.5	70	52	63
13	6.5	32.5	100	47.2	57.1
14	6.5	32.5	70	49	61
15	3.824284	48.851598	52.161893	70	79.6
16	11	32.5	70	1.2	3.4
17	6.5	32.5	40	55	63.2
18	6.5	60	70	60.4	69.5
19	6.5	32.5	70	52.7	62.8
20	9.175716	48.851598	52.161893	17.1	18.5

Table 2
Design of experience–effect of salt in adsorption

RUN	Salt	Time	DR23 $CaCl_2$	DR80 $CaCl_2$	DR23 Na_2SO_4	DR80 Na_2SO_4
1	2.7071068	51.213203	74.59	82.21	79.21	87.21
2	2	60	74.66	82.28	79.25	87.28
3	1.2928932	51.213203	74.03	82.01	79.14	87.01
4	2	30	72	80	77	85
5	1	30	71	79	76	84
6	2	5	53	67.5	58	72.5
7	1.2928932	8.7867966	65	60	58.5	65
8	3	30	73	81	78	86
9	2	30	72.01	80.1	77	85.1
10	2	30	72	80	76.99	85
11	2	30	71.98	80.05	77.01	85.05
12	2	30	72	80.03	77.02	85.03
13	2.7071068	8.7867966	66	63	59	68

particular set of mathematical and statistical methods which is utilized for designing experiments, evaluating the effects of variables and finding optimum conditions of variables to predict targeted responses [36–38]. Also, the formulation of new products and optimizing their performance can be improved by this method. Here DR23, DR80, pH, dye concentration and time are control variables and optimization of process conditions is the main variable.

Hypotheses: pH, dye concentration, time, and salt have a significant effect on the optimization of DR23 adsorption by PAMAM grafted PAN-DETA.

H_0: pH, dye concentration, and time have not a significant effect on the optimization of DR23 adsorption by PAMAM grafted PAN-DETA.

H_1: pH, dye concentration, and time have a significant effect on the optimization of DR23 adsorption by PAMAM grafted PAN-DETA.

H_0: reliability > 0.05

H_1: reliability ≤ 0.05

3. Results and discussion

3.1. ATR-FTIR study of functionalized PAN and surface modified PAN nanofiber

The chemical changes occurred in the PAN/DETA nanofibers were investigated in our previous study by FTIR analysis [35]. It was found that the addition of DETA compound to the PAN matrix results to form or introduce many OH and NH groups in the PAN nanofibers. Also, the nitrile group of PAN polymer was changed to amidine group (N–C=N) and crosslinking of PAN polymers occurred in the polymer matrix [35].

The ATR-FTIR spectra of PAN-DETA and PAMAM surface grafted PAN-DETA nanofiber mats are shown in Fig. 2. PAN-DETA spectrum (curve a) showed several peaks at 3,440,

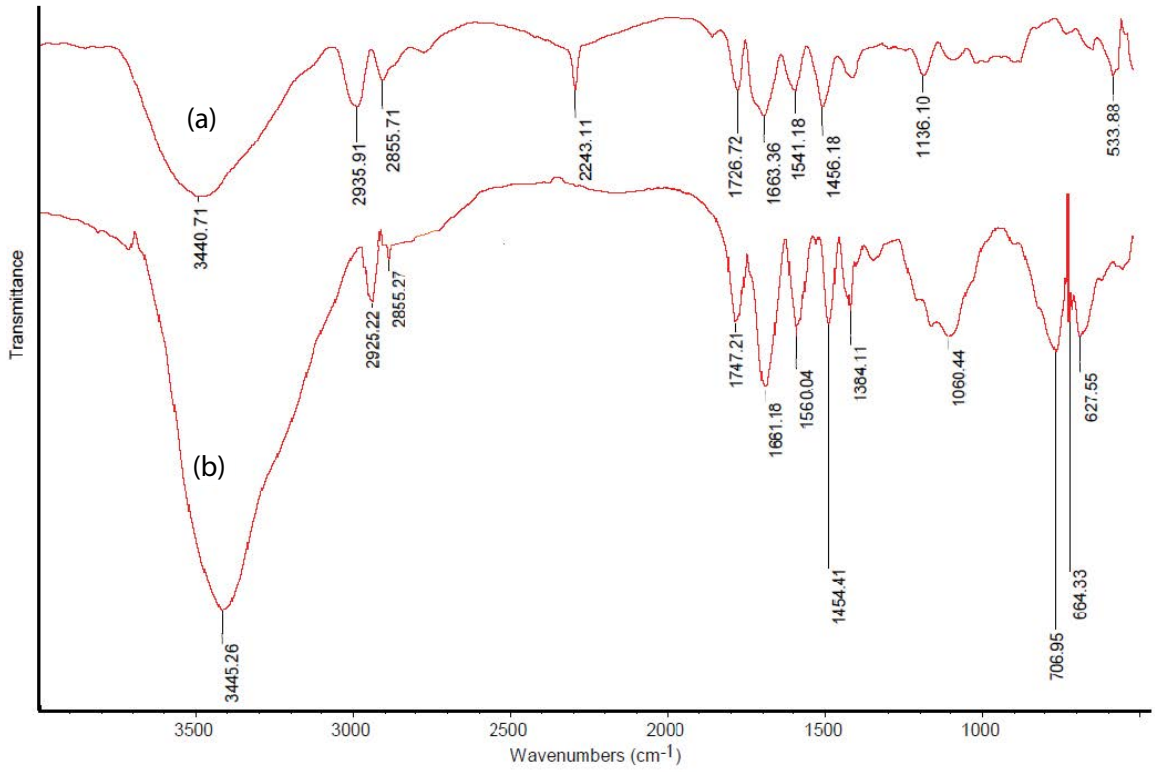

Fig. 2. ATR spectra of (a) PAN-DETA nanofibers, and (b) PAMAM surface grafted PAN-DETA nanofibers.

2,243, 1,663, 1,541, and 1,456 cm^{-1}, attributing to the stretching vibrations of NH overlapped with OH groups, nitrile groups, amidine groups, bending vibrations of the secondary amine and methyl groups of DETA, respectively. As can be seen in Fig. 3(b), for the PAMAM surface grafted PAN nanofiber, there is not a significant change in peaks compared with PAN-DETA mat except the changes in the intensity of the bands at 3,445, 1,661, 1,560 cm^{-1} relating to the stretching vibration of NH_2, overlapping of amidine and imine groups, as well as the bending vibrations of the secondary amines, respectively. Furthermore, an increase in the intensity of C=O band at 1,747cm^{-1} was observed due to grafting PAMAM on the PAN-DETA nanofiber. Based on FTIR and ATR results, a mechanism can be proposed for the reaction between PAN-DETA nanofiber and PAMAM by using glutaraldehyde as the crosslinking agent according to Fig. 3.

3.2. Evaluation of morphology of samples by SEM

Fig. 4 shows the SEM images of untreated PAN, PAN-DETA, and PAMAM grafted PAN-DETA nanofiber. SEM images clearly showed that the surface of PAN-DETA nanofiber (Fig. 4(b)) is rougher and irregular compared to untreated PAN due to alkali treatment (see AFM

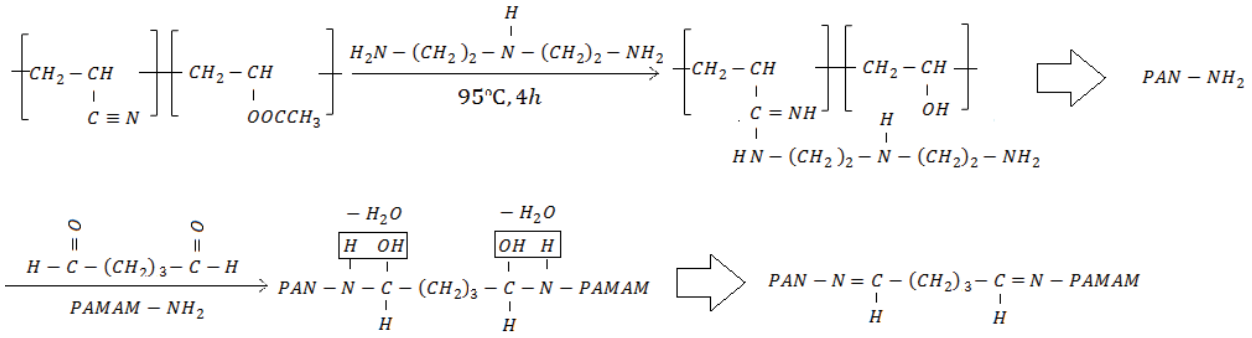

Fig. 3. Proposed mechanism for the reaction between PAN-DETA nanofibers and PAMAM by using glutaraldehyde.

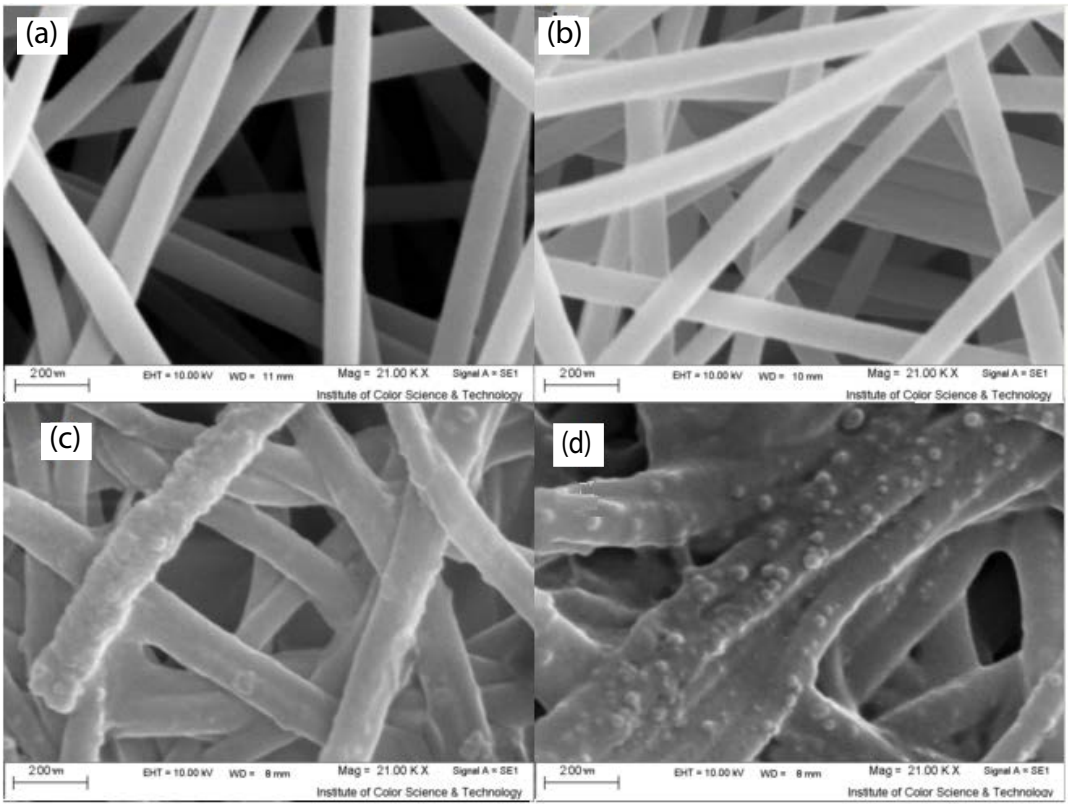

Fig. 4. SEM images of (a) untreated PAN nanofiber, (b) PAN-DETA nanofiber, (c) PAMAM grafted PAN-DETA nanofiber (deposition of a dense layer on the nanofibers surface), and (d) PAMAM grafted PAN-DETA nanofiber (formation of nanoparticles on the nanofibers surface and attaching of nanofibers together).

analysis). PAMAM grafted PAN-DETA image showed the formation of a dense layer on the surface of nanofiber (Fig. 4(c)).In addition, the images showed the formation of some nanoparticles among the deposited layer. These nanoparticles are probably generated through crosslinking of some PAMAM molecules by excess glutaraldehyde molecules (Fig. 4(d)). The glutaraldehyde role can be described as following: (a) It makes a connection between the amine groups of PAMAM and amine groups of PAN-DETA nanofiber, (b) crosslinking of nanofibers together by making the connection between amine groups of nanofibers (Fig. 4(e)), (c) creation of nanoparticle through crosslinking of PAMAM molecules with glutaraldehyde on nanofiber surface. The average diameter of nanofibers increased from 220 for untreated PAN nanofiber to 230 for PAN-DETA nanofiber and 320 nm for PAMAM grafted PAN-DETA nanofiber. Increasing in nanofibers diameters can be due to swelling of nanofiber after the functionalization process and formation of a layer on the nanofibers surface after the grafting process.

Fig. 5 presents pore size distribution curves of nanofibers obtained by the BJH method. The result indicated a relatively narrow pore size distribution for untreated PAN and PAN-DETA nanofiber centered at about 450, 500 nm, respectively, and a wide distribution for PAMAM grafted PAN-DETA nanofiber centered at 700 nm. In addition, a BET analysis revealed that the surface area of various nanofibers decreased from 30.4 for untreated PAN to 27.8 and 14 $m^2 g^{-1}$ for PAN-DETA and PAMAM grafted PAN-DETA nanofiber, respectively. Increasing the average pore size and decreasing the total surface area values are because of increasing the nanofiber diameter [39]. The porosity of electrospun nanofibers ranged from 25% to 65% for average diameter of 220–320 nm.

3.3. AFM analysis

Fig. 6 showed the AFM images the untreated PAN, PAN-DETA, and PAMAM grafted PAN-DETA nanofibers. AFM gives a three-dimensional image of the surface; hence, it is a useful technique for the investigation of surface topographies and evaluation of the surface roughness of a sorbent [27]. The average roughness (Sa) of the surfaces can be calculated from the roughness profile determined from the AFM images. For the untreated PAN, PAN-DETA, and PAMAM grafted PAN-DETA nanofibers the values of Sa were 42.4, 46.4, and 68.6–81.9 nm, respectively, which indicates that the surfaces of the PAN nanofiber became rough after the functionalization and grafting process of the PAN nanofiber. An increment in average roughness value after the grafting process indicates successful grafting of PAMAM on the surface of functionalized PAN nanofiber. Furthermore, the results presented a variation in the roughness values for PAMAM grafted PAN-DETA nanofiber. The variation of average roughness values can be due to the formation of a dense and non-uniform layer on the surface of nanofibers. Also, the conglutination of nanofibers can be another reason for the variation of surface roughness.

3.4. Optimization of dye removal condition

Three operating parameters for dye removal viz., time, dye concentration and pH have been optimized by RSM using Design Expert software version 7.0.0.1 (Fig. 7 and Tables 3 and 4). Given that the reliability is less than 0.5 in the RSM model. Therefore, there is a significant difference between the effects of variables on adsorption. In this regard, H_0 is rejected and H_1 is accepted. Hence it can be concluded that pH, dye concentration and time have a significant effect on the optimization of DR23 adsorption by PAMAM grafted PAN-DETA. Also, since the test statistic of *F*-value is greater than the model statistic in pH, so pH variable is more effective in dye adsorption.

In the adsorption of DR80, it was deduced that H_0 rejected and H_1 accepted. Hence it can be concluded that pH, dye concentration and time have a significant effect on the optimization of DR80 adsorption by PAMAM grafted

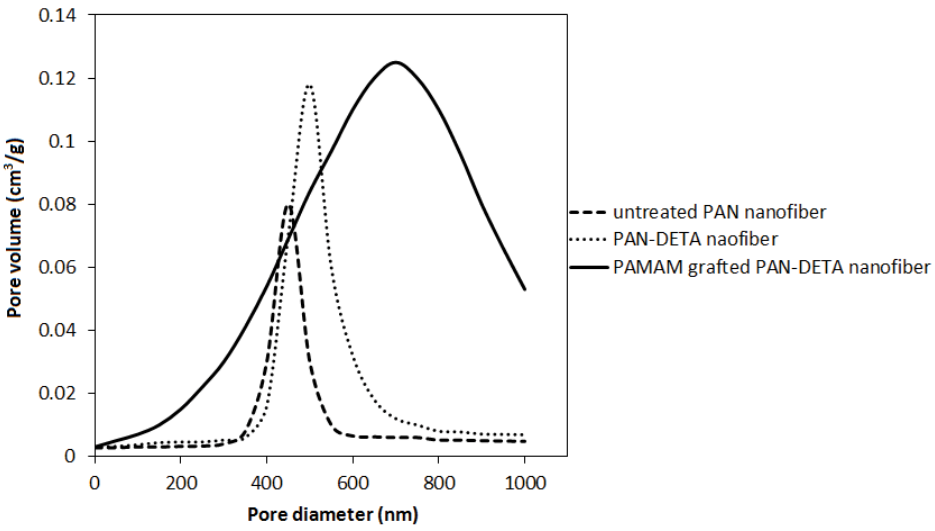

Fig. 5. Pore size distribution curves of nanofibers.

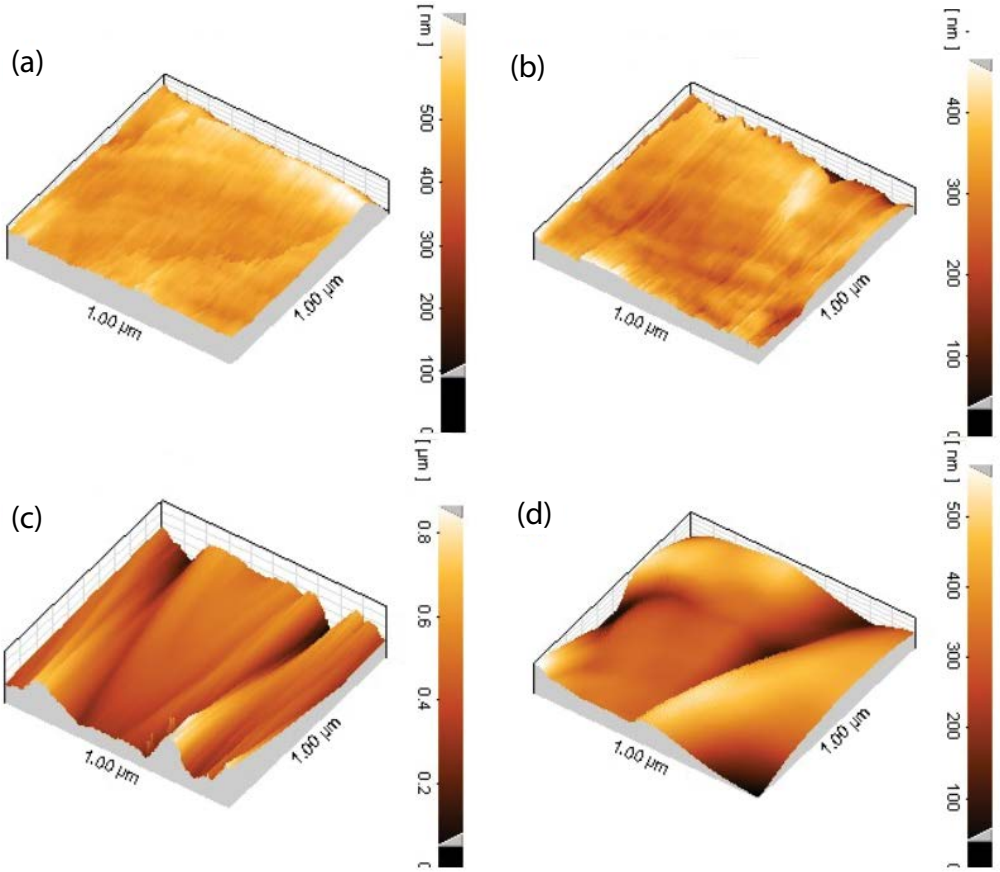

Fig. 6. AFM images of (a) untreated PAN nanofiber, (b) PAN-DETA nanofiber, (c) PAMAM grafted PAN-DETA nanofiber (surface average roughness = 81.9 nm), and (d) PAMAM grafted PAN-DETA nanofiber (surface average roughness = 68.6 nm).

PAN-DETA. Also, the test statistic of *F*-value is greater than the model statistic in pH, so pH variable is more effective in dye adsorption.

On the basis of the results obtained from the surface plots and the independent variables (Tables 5–14), several mathematic equations were presented for the prediction of each response Eqs. (2)–(7).

$$\begin{aligned}\text{DR23} = {} & +91.46868 + 8.54336 \times [\text{pH}] + 0.62887 \times [\text{Time}] - 1.65565 \times \\ & [\text{Concentration}] - 0.016599 \times [\text{pH}] \times [\text{Time}] + 0.13914 \times \\ & [\text{pH}] \times [\text{Concentration}] + 4.58548E - 004 \times [\text{Time}] \times \\ & [\text{Concentration}] - 1.76937 \times [\text{pH}]^2 - 4.27076E - 003 \times \\ & [\text{Time}]^2 + 2.96693E - 003 \times [\text{Concentration}]^2\end{aligned} \tag{2}$$

$$\begin{aligned}\text{DR80} = {} & +46.74820 + 13.60203 \times [\text{pH}] + 1.36678 \times [\text{Time}] - 0.81735 \times \\ & [\text{Concentration}] - 0.035455 \times [\text{pH}] \times [\text{Time}] + 0.13862 \times \\ & [\text{pH}] \times [\text{Concentration}] - 2.8841E - 003 \times [\text{Time}] \times \\ & [\text{Concentration}] - 2.16840 \times [\text{pH}]^2 - 9.73233E - \\ & 003 \times [\text{Time}]^2 - 2.17786E - 003 \times [\text{Concentration}]^2\end{aligned} \tag{3}$$

$$\begin{aligned}\text{DR23 CaCl}_2 = {} & +59.20242 - 5.44724 \times [\text{Salt}] + 0.83271 \times [\text{Time}] - \\ & 7.33333E - 003 \times [\text{Salt}] \times [\text{Time}] + 1.61075 \times \\ & [\text{Salt}]^2 - 8.48698E - 003 \times [\text{Time}]^2\end{aligned} \tag{4}$$

$$\begin{aligned}\text{DR80 CaCl}_2 = {} & +42.76856 + 11.65179 \times [\text{Salt}] + 1.23931 \times [\text{Time}] - \\ & 0.046667 \times [\text{Salt}] \times [\text{Time}] - 2.29653 \times \\ & [\text{Salt}]^2 - 0.012125 \times [\text{Time}]^2\end{aligned} \tag{5}$$

$$\begin{aligned}\text{DR23 Na}_2\text{SO}_4 = {} & + 43.59836 + 5.52452 \times [\text{Salt}] + 1.35278 \times [\text{Time}] - \\ & 7.16667E - 003 \times [\text{Salt}] \times [\text{Time}] - 1.17719 \times \\ & [\text{Salt}]^2 - 0.014425 \times [\text{Time}]^2\end{aligned} \tag{6}$$

$$\begin{aligned}\text{DR80 Na}_2\text{SO}_4 = {} & + 47.76856 + 11.65179 \times [\text{Salt}] + 1.23931 \times [\text{Time}] - \\ & 0.046667 \times [\text{Salt}] \times [\text{Time}] - 2.29653 \times [\text{Salt}]^2 - \\ & 0.012125 \times [\text{Time}]^2\end{aligned} \tag{7}$$

3.5. Adsorption studies

3.5.1. Effect of adsorbent dosage

The effect of adsorbent dosage on the removal of DR80 and DR23 from solution is shown in Fig. 8. For an adsorbent

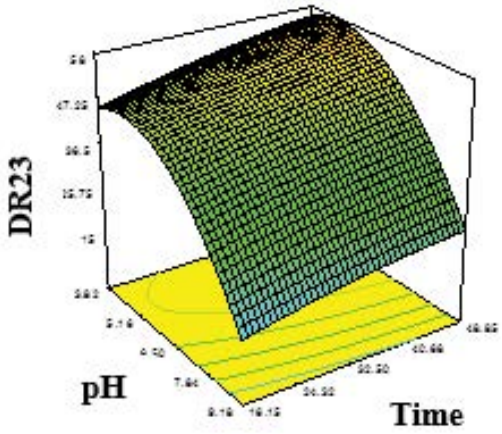

(a)

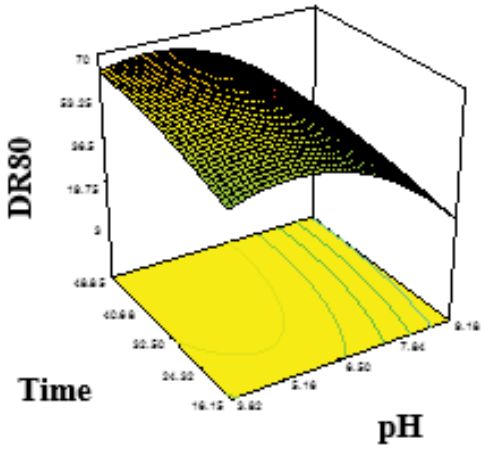

(b)

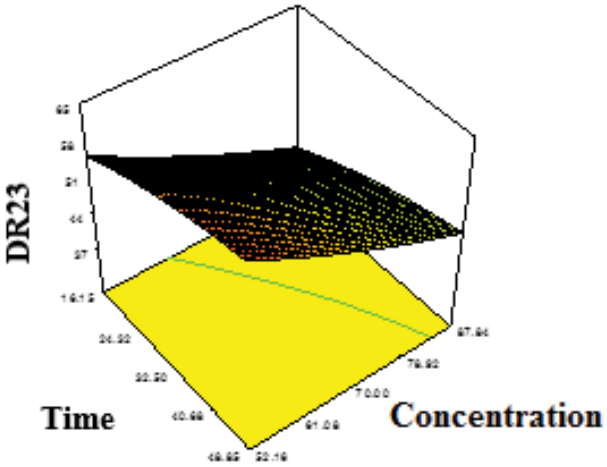

(c)

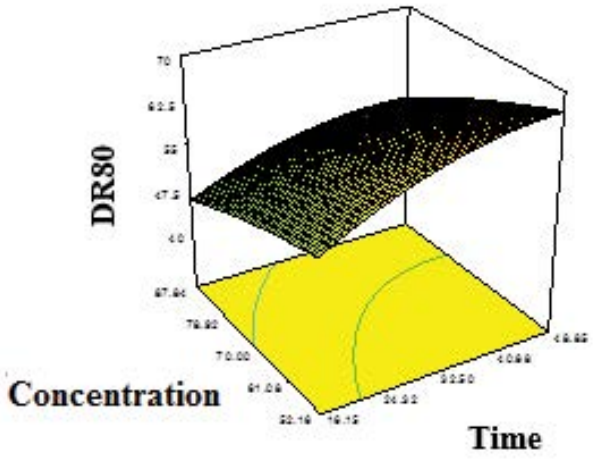

(d)

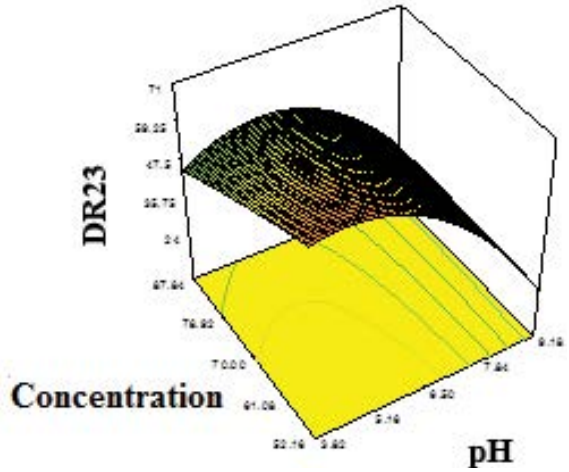

(e)

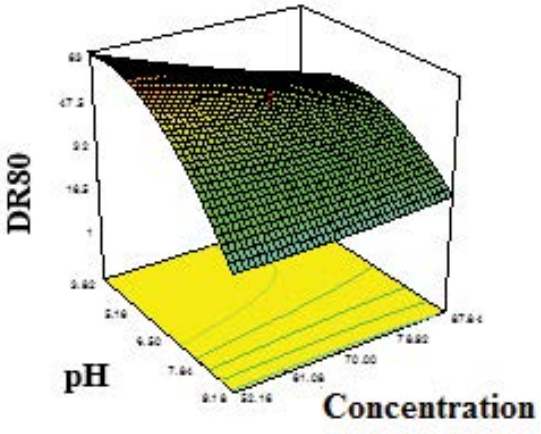

(f)

Fig. 7.–(*Continued*)

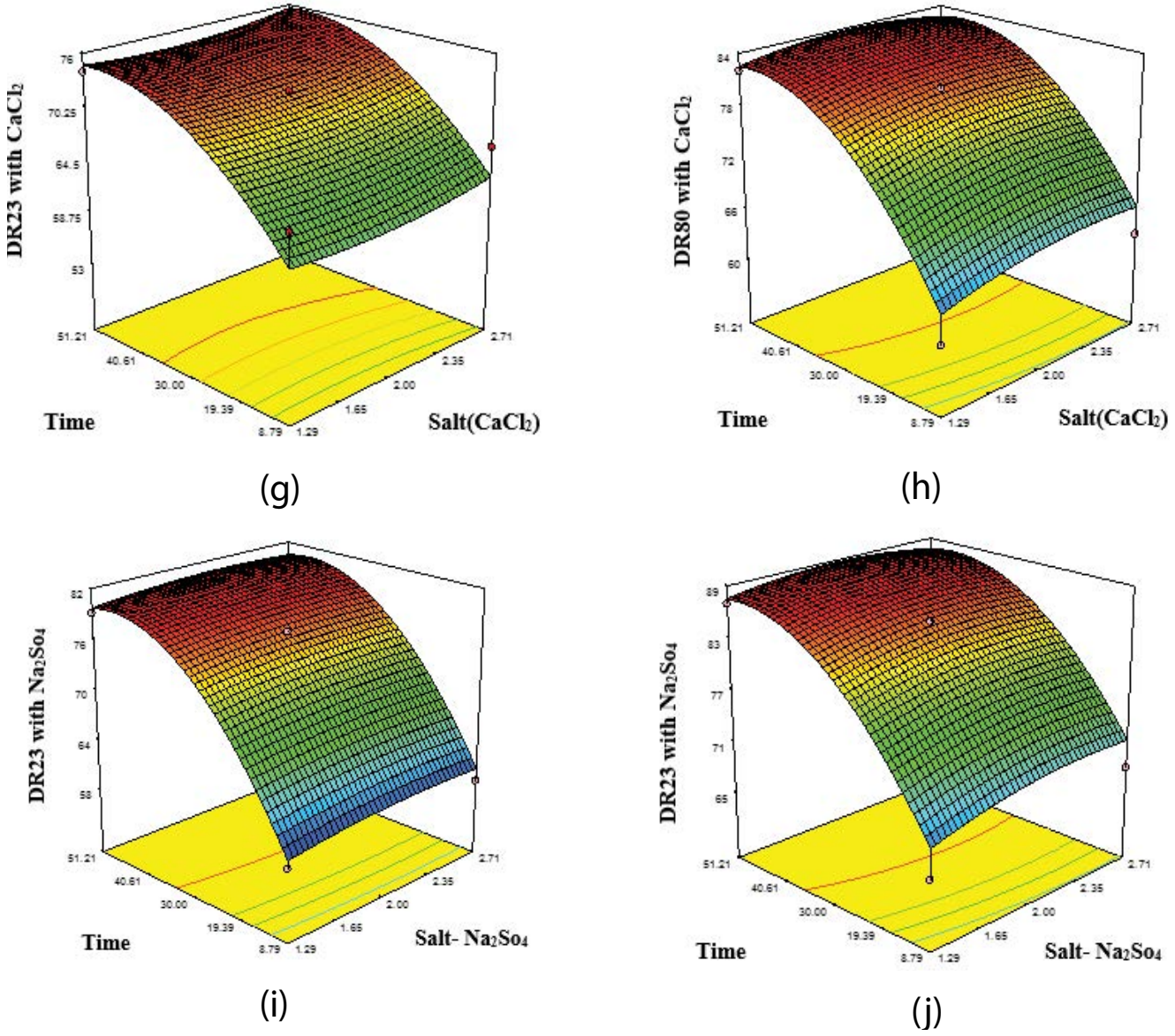

Fig. 7. (a) model of pH and time effect on DR23 adsorption, (b) model of pH and time effect on DR80 adsorption, (c) model of time and dye concentration effect on DR23 adsorption, (d) model of time and dye concentration effect on DR80 adsorption, (e) model of dye concentration and pH effect on DR23 adsorption, (f) model of dye concentration and pH on DR80 adsorption, (g) model of time and $CaCl_2$ effect on DR23 adsorption, (h) model of time and $CaCl_2$ on DR80 adsorption, (i) model of time and Na_2SO_4 effect on DR23 adsorption, and (j) model of time and Na_2SO_4 on DR80 adsorption.

to be efficient in wastewater treatment, it needs to be able to show a rapid uptake of the pollutants and reach the equilibrium in a short time. As can be seen, the adsorption process was initially rapid and then it slowed down, reached the equilibrium. Rapid adsorption of dyes at the initial minutes is due to a great number of vacant adsorption sites existing for interaction with dyes [40] and the high concentration of dye. Adsorption rate was after further treatment decreased due to saturation of the adsorptive sites as well as a decrease in the dye concentration.

With increasing the adsorbent dosage, the adsorption percent increases but adsorption capacity decreases. An increase in adsorption percent can be attributed to more available adsorption sites at the surface of the fibers, whereas the decrease in adsorption capacity is due to remain some of the adsorption sites unsaturated during the adsorption process.

3.5.2. Effect of pH

In general, the final dye concentration of solution after adsorption by the adsorbent varies significantly with the initial pH of dye solutions. The effect of initial pH on dye removal of DR80 and DR23 is shown in Fig. 9. As can be

Table 3
ANOVA analysis of variance for response surface optimization model of pH, concentration dye, and time effect on DR23 adsorption

ANOVA for Response Surface Quadratic Model						
Analysis of variance table [Partial sum of squares - Type III]						
	Sum of		Mean	*F*	*p*-value	
Source	Squares	*df*	Square	Value	Prob > *F*	
Model	6,168.32	9	685.37	7.05	0.0026	significant
A-pH	2,703.1	1	2,703.1	27.81	0.0004	
B-time	277.1	1	277.1	2.85	0.1222	
C-con	447.64	1	447.64	4.61	0.0575	
AB	4.22	1	4.22	0.043	0.8391	
AC	352.85	1	352.85	3.63	0.0859	
BC	0.14	1	0.14	1.47E-03	0.9701	
A^2	2,312.6	1	2,312.6	23.79	0.0006	
B^2	18.79	1	18.79	0.19	0.6695	
C^2	12.84	1	12.84	0.13	0.7238	
Residual	972.06	10	97.21			
Lack of fit	829.85	5	165.97	5.84	0.0377	significant
Pure error	142.21	5	28.44			
Cor. total	7,140.37	19				

Table 4
ANOVA analysis of variance for response surface optimization model of pH, concentration dye and time effect on DR80 adsorption

ANOVA for Response Surface Quadratic Model						
Analysis of variance table [Partial sum of squares - Type III]						
	Sum of		Mean	*F*	*p*-value	
Source	Squares	*df*	Square	Value	Prob > *F*	
Model	8,204.05	9	911.56	8.76	0.0011	Significant
A-pH	3,562.43	1	3,562.43	34.25	0.0002	
B-Time	332.66	1	332.66	3.2	0.104	
C-con	431.09	1	431.09	4.14	0.0691	
AB	19.25	1	19.25	0.19	0.6762	
AC	350.2	1	350.2	3.37	0.0964	
BC	5.66	1	5.66	0.054	0.8202	
A^2	3,473.29	1	3,473.29	33.39	0.0002	
B^2	97.58	1	97.58	0.94	0.3556	
C^2	6.92	1	6.92	0.067	0.8017	
Residual	1,040.17	10	104.02			
Lack of fit	920.54	5	184.11	7.69	0.0214	significant
Pure error	119.63	5	23.93			
Cor total	9,244.22	19				

seen, the maximum adsorption of both dyes occurred at pH = 3.5 due to a high electrostatic attraction between the positively charged surface of nanofiber and anionic dye molecules. It is reported that PAMAM dendrimer has primary amine groups on the surface (*pKa* = 6.85) [41], confirming that the adsorbent surface bears a positive charge at pH = 3.5. As the pH of a system increases, the number of negatively charged sites increases. A negatively charged site on the adsorbent does not favor the adsorption of anionic dyes due to electrostatic repulsion [42]. The competition between OH^- ions and dye molecules is a reason for decreasing dye removal at alkaline pH. As can be seen from the figure, the amount of dye removal percentages decreased when the pH of the solution decreased from 3 due to breakage of imine bonds connected the PAMAM molecule to the PAN-DETA nanofiber by glutaraldehyde. After the breakage of the imine

Table 5
ANOVA analysis of variance for response surface optimization model of $CaCl_2$ salt effect on DR23 adsorption

ANOVA for Response Surface Quadratic Model						
	Sum of		Mean	*F*	*p*-value	
Source	Squares	*df*	Square	Value	Prob > *F*	
Model	356.45701	5	71.291402	7.9969175	0.0082	Significant
A-$CaCl_2$	2.4072866	1	2.4072866	0.2700308	0.6193	
B-time	308.54204	1	308.54204	34.609857	0.0006	
AB	0.0484	1	0.0484	0.0054291	0.9433	
A^2	4.5562693	1	4.5562693	0.511087	0.4978	
B^2	80.786978	1	80.786978	9.0620578	0.0197	
Residual	62.404022	7	8.9148602			
Lack of fit	62.403542	3	20.801181	173343.17	< 0.0001	Significant
Pure error	0.00048	4	0.00012			

Table 6
ANOVA analysis of variance for response surface optimization model of $CaCl_2$ salt effect on DR80 adsorption

ANOVA for Response Surface Quadratic Model						
	Sum of		Mean	*F*	*p*-value	
Source	Squares	*df*	Square	Value	Prob > *F*	
Model	662.01289	5	132.40258	15.889049	0.0011	Significant
A-$CaCl_2$	4.5427417	1	4.5427417	0.5451544	0.4843	
B-time	566.56212	1	566.56212	67.99062	< 0.0001	
AB	1.96	1	1.96	0.2352109	0.6425	
A^2	9.2617694	1	9.2617694	1.11E+00	0.3268	
B^2	164.88842	1	164.88842	19.787532	0.0030	
Residual	58.330618	7	8.3329454			
Lack of fit	58.323698	3	19.441233	11237.707	< 0.0001	Significant
Pure error	0.00692	4	0.00173			
Cor total	7.20E + 02	12				

Table 7
ANOVA analysis of variance for response surface optimization model of Na_2SO_4 salt effect on DR23 adsorption

ANOVA for Response Surface Quadratic Model						
	Sum of		Mean	*F*	*p*-value	
Source	Squares	*df*	Square	Value	Prob > *F*	
Model	848.46412	5	169.69282	103.07722	< 0.0001	Significant
A-Na_2SO_4	1.4436634	1	1.4436634	0.8769304	0.3802	
B-time	723.66215	1	723.66215	439.57711	< 0.0001	
AB	0.046225	1	0.046225	0.0280786	0.8717	
A^2	2.4335711	1	2.4335711	1.4782342	0.2635	
B^2	233.37269	1	233.37269	141.75854	< 0.0001	
Residual	11.523883	7	1.646269			
Lack of fit	11.523363	3	3.8411209	29,547.084	< 0.0001	Significant
Pure error	0.00052	4	0.00013			
Cor total	859.988	12				

Table 8
ANOVA analysis of variance for response surface optimization model of Na_2SO_4 salt effect on DR80 adsorption

ANOVA for Response Surface Quadratic Model						
	Sum of		Mean	*F*	*p*-value	
Source	Squares	*df*	Square	Value	Prob > *F*	
Model	662.01289	5	132.40258	15.889049	0.0011	Significant
A-Na_2SO_4	4.5427417	1	4.5427417	0.5451544	0.4843	
B-time	566.56212	1	566.56212	67.99062	< 0.0001	
AB	1.96	1	1.96	0.2352109	0.6425	
A^2	9.2617694	1	9.2617694	1.1114641	0.3268	
B^2	164.88842	1	164.88842	19.787532	0.0030	
Residual	58.330618	7	8.3329454			
Lack of fit	58.323698	3	19.441233	11237.707	< 0.0001	Significant
Pure error	0.00692	4	0.00173			
Cor total	720.34351	12				

Table 9
Optimal conditions of software for pH, dye concentration and time use in DR23 adsorption by PAMAM grafted PAN-DETA (95% confidence level)

Number	pH	Time	Concentration	DR23	Desirability
1	4.32	48.85	52.16	66.6137	0.955

Table 10
Optimal conditions of software for pH, dye concentration and time use in DR80 adsorption by PAMAM grafted PAN-DETA (95% confidence level)

Number	pH	Time	Concentration	DR80	Desirability
1	4.32	48.85	52.16	76.4299	0.955

Table 11
Optimal conditions of software for $CaCl_2$ salt use in DR23 adsorption by PAMAM grafted PAN-DETA (95% confidence level)

Number	Salt ($CaCl_2$)	Time	DR23	Desirability
1	2.23	46.16	74.6639	1.000

Table 12
Optimal conditions of software for $CaCl_2$ salt use in DR80 adsorption by PAMAM grafted PAN-DETA (95% confidence level)

Number	Salt ($CaCl_2$)	Time	DR80	Desirability
1	2.47	41.66	74.7804	1.000

Table 13
Optimal conditions of software for Na_2SO_4 salt use in DR23 adsorption by PAMAM grafted PAN-DETA (95% confidence level)

Number	Salt (Na_2So_4)	Time	DR23	Desirability
1	2.31	47.92	83.8044	1.000

Table 14
Optimal conditions of software for Na_2SO_4 salt use in DR80 adsorption by PAMAM grafted PAN-DETA (95% confidence level)

Number	Salt (Na_2SO_4)	Time	DR80	Desirability
1	2.50	45.81	83.5185	1.000

bonds, a large number of dye molecules adsorbed to the PAMAM molecule existing in the dye solution and cannot be separated by nanofiber mat. The reason for increasing the adsorption efficiency at lower pH value can be explained by IEP. As mentioned earlier, the IEP of PAMAM grafted nanofibers was 5.1. Decreasing the IEP value from 6 (for PAN-DETA nanofibers) 5.1 for grafted nanofibers was due to the presence of amine groups on the surface. At the pH values lower than IEP, the positive charge creates on the surface. Also, at the pH values higher than IEP, the nanofiber surface bears a negative charge [43]. At the pH of 3.5, the charged surface of nanofibers was positive due to protonation of amine groups. Positively charged adsorbent interacts with the negatively charged dye molecules (due to the existence of sulfonic and hydroxyl groups in their structure that confer low *pKa* values). Previously, $pK < 1$ for DR80 dye (due to the presence of six sulfonic acid) was reported by researchers [44].

3.5.3. Effect of initial dye concentration

The effect of initial dye concentration of DR80 and DR23 on dye removal of PAMAM surface grafted PAN-DETA nanofiber is shown in Fig. 10. The amount of the dye adsorbed onto the surface of nanofiber increases with an increase in the initial dye concentration of solution. This can be due to an increase in the driving force of the concentration gradient at the higher initial dye concentration [45]. In addition, increase of initial dye concentration increases the number of collisions between dye anions and adsorbent, which enhances the sorption process. In the case of lower concentrations, the ratio of initial dye molecules to the available adsorption sites is low and subsequently the fractional adsorption becomes independent from the initial concentration [46,47]

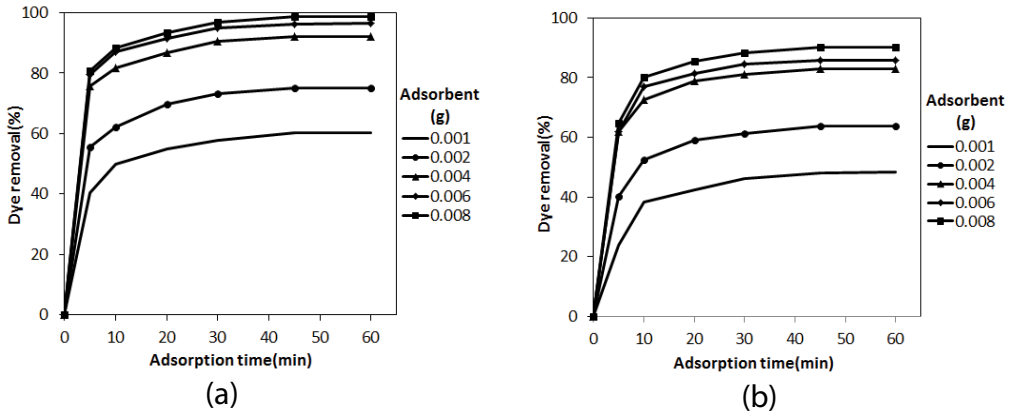

Fig. 8. Effect of adsorbent dosage on the dye removal in different times, (a) DR80, and (b) DR23.

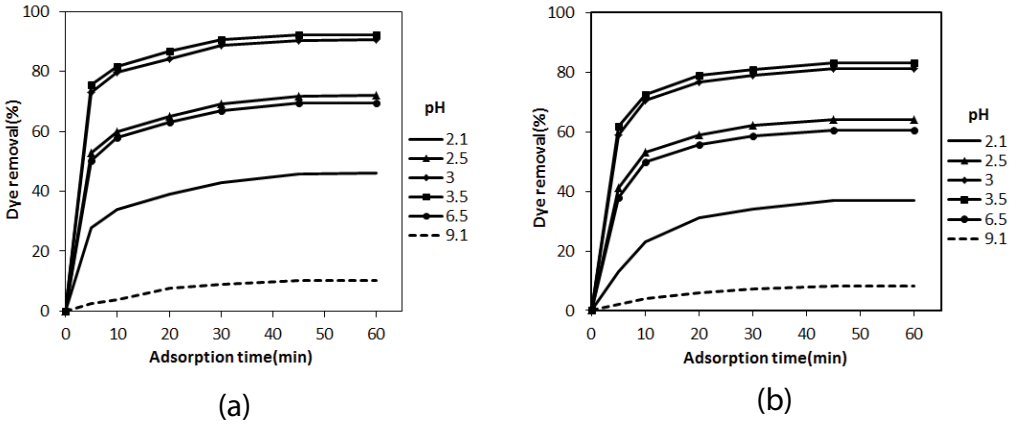

Fig. 9. Effect of pH on dye removal in different times, (a) DR80, and (b) DR23.

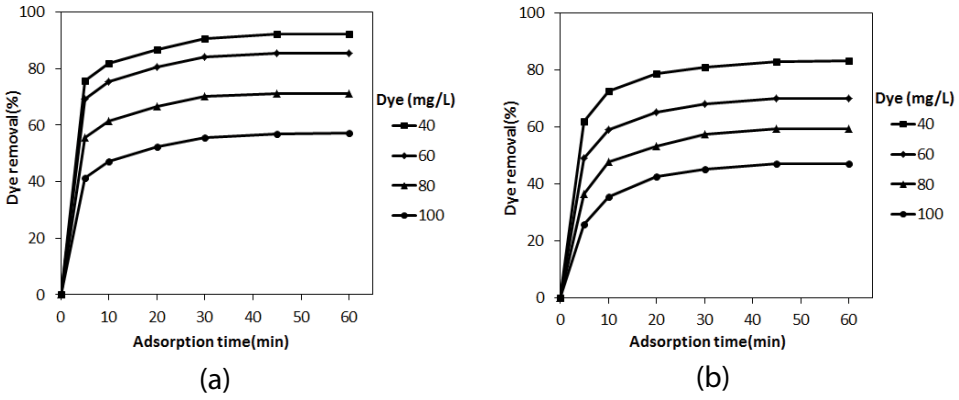

Fig. 10. Effect of the initial dye concentration on dye removal in different times, (a) DR80, and (b) DR23.

3.5.4. Effect of ionic strength (salts)

The effect of ionic strength (salts) on dye adsorption was evaluated and the results are shown in Fig. 11. The addition of salts into the dye solutions slightly decreased the adsorption efficiency of nanofibers which was assigned to the formation of a complex between anionic dyes and salt cations (Figs. 11(a) and (b)). Also, the neutralization or screening of cationic sites of the adsorbent by salt anions was regarded as another reason for this phenomenon [18]. Also, anions have small sizes and compete with dyes in adsorption process resulted in decreasing the adsorption capacity [19]. According to the figure, the adsorption efficiency showed a higher decrease for $CaCl_2$ compared to Na_2SO_4 which was attributed

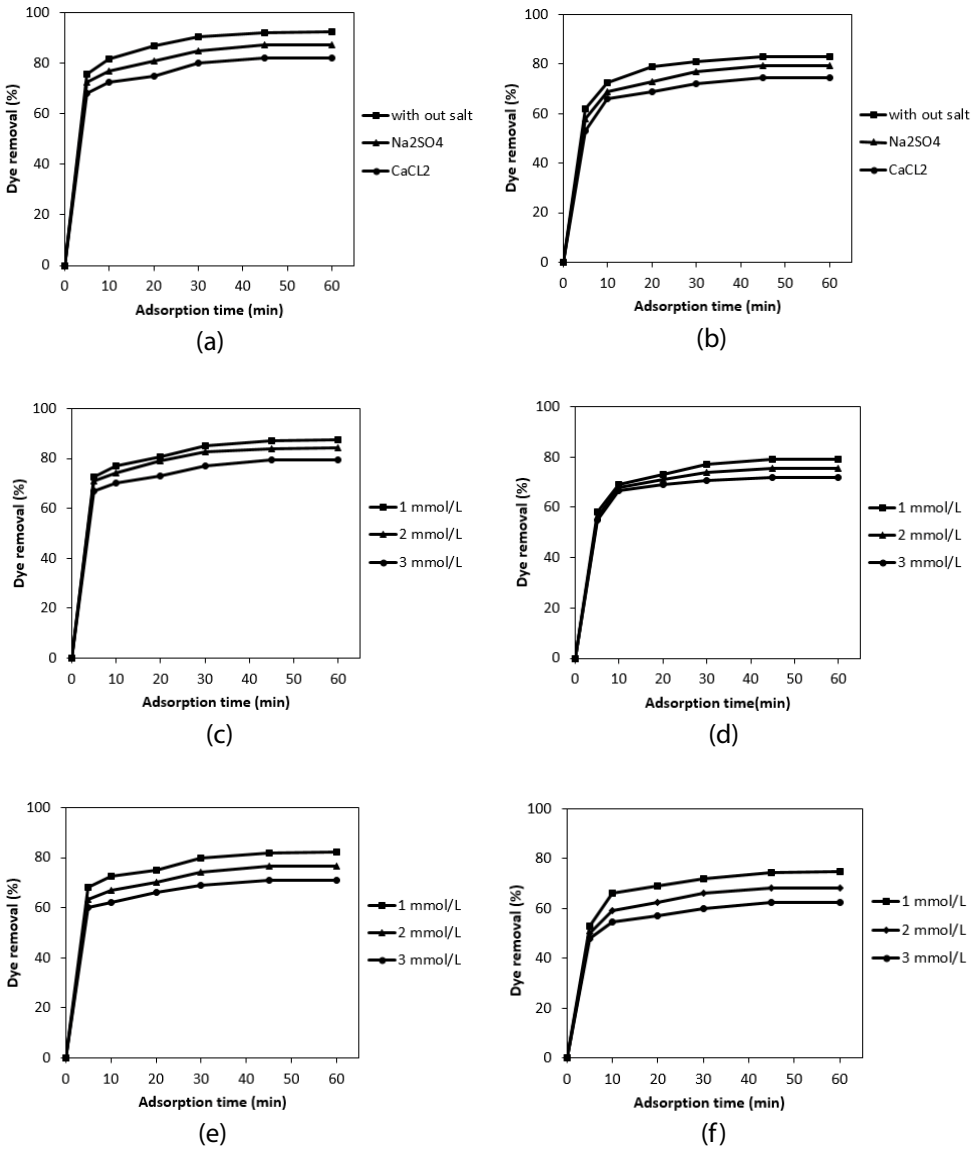

Fig. 11. Effect of the ionic strength (salts)on dye removal in different times, (a) DR80, 1 mmol/L salt, pH = 3.5, 40 ppm, (b) DR23, 1 mmol/L salt, pH = 3.5, 40 ppm, (c) DR80, Na_2SO_4 salt, pH = 3.5, 40 ppm, (d) DR23, Na_2SO_4 salt, pH = 3.5, 40 ppm, (e) DR80, $CaCl_2$ salt, pH = 3.5, 40 ppm, and (f) DR23, $CaCl_2$ salt, pH = 3.5, 40 ppm.

to the coordination of the Ca^{2+} ions with the anionic dyes. Evaluating the effect of salt concentration on dye removal revealed that the adsorption efficiency was decreased with raising the salt content which can be due to the higher amount of formed complexes of salt cations and dye anions. On the other hand, with increasing the number of salts in the solution the solubility of dyes was decreased because, after the addition of salts, the dissociation of dye molecules to the ionic forms decreases and also polarity of the solution increases resulted to remain dye molecules as dominant species.

3.5.4. Adsorption isotherms

Adsorption isotherms indicate the relation between the mass of dye adsorbed at constant temperature per unit mass of adsorbent and liquid phase dye concentration at equilibrium. They present the dye distribution between the liquid and solid phases at various equilibrium concentrations. Adsorption isotherms give information of the adsorption system progress and indicate interaction of an adsorbent with adsorbate [48]. Several isotherms such as Langmuir, Freundlich, and Temkin models were studied in literature to describe the experimental data of adsorption. A basic assumption of the Langmuir theory is that sorption takes place at specific sites within the adsorbent [49,50].

The Langmuir equation can be written as follows [51,52]:

$$q_e = \frac{Q_0 K_L C_e}{1 + K_L C_e} \tag{8}$$

where q_e, C_e, K_L, and Q_0 are the amount of dye adsorbed on adsorbent at equilibrium (mg g^{-1}), the equilibrium

concentration of dye solution (mg L^{-1}), Langmuir constant (L g^{-1}) and the maximum adsorption capacity (mg g^{-1}), respectively.

The linear form of Langmuir equation is:

$$\frac{C_e}{q_e} = \frac{1}{K_L Q_0} + \frac{C_e}{Q_0} \tag{9}$$

Another isotherm for consideration is Freundlich. The basic assumption of this model is that there is an exponential variation in site energies of adsorbent, and also surface adsorption is not a rate limiting step [53]. The Freundlich isotherm is derived by assuming a heterogeneous surface with a non-uniform distribution of adsorption heat over a surface. Such a result can be expressed by [54]:

$$q_e = K_F C_e^{1/n} \tag{10}$$

where K_F is the adsorption capacity at unit concentration and $1/n$ is the adsorption intensity.

$1/n$ values indicate the type of isotherm to be irreversible ($1/n=0$), favorable ($0<1/n<1$) and unfavorable ($1/n>1$). Eq. (11) can be rearranged to a linear form:

$$\log q_e = \log K_F + \frac{1}{n}\log C_e \tag{11}$$

The Temkin isotherm contains a factor that considers the adsorbing species and adsorbent interactions. The Temkin isotherm assumes that the heat of adsorption of all the molecules in the layer decreases linearly with coverage due to adsorbent-adsorbate interactions. In this isotherm, the adsorption is described by a uniform distribution of binding energies, up to some maximum binding energy [55].

The Temkin isotherm is given as:

$$q_e = \frac{RT}{b\ln\left(K_T C_e\right)} \tag{12}$$

Linearized form of Eq. (12) is written as:

$$q_e = B_1 \ln K_T + B_1 \ln C_e \tag{13}$$

where

$$B_1 = \frac{RT}{b} \tag{14}$$

K_T is the equilibrium binding constant (L mol^{-1}) corresponding to the maximum binding energy and constant B_1 is related to the heat of adsorption. T is also the absolute temperature (K), and R is the universal gas constant (8.314 J mol^{-1} K^{-1}).

In this study, in order to determine the constants in Langmuir, Freundlich, and Temkin isotherms, a plot of C_e/q_e vs. C_e, $\log q_e$ vs. $\log C_e$, and q_e vs. ln C_e were drawn. The coefficient values for various isotherms are shown in Table 15.

The R^2 values showed that the dye removal isotherm using PAMAM surface grafted PAN-DETA nanofiber did not follow the Freundlich and Temkin isotherms (Table 15). R^2 value for Langmuir isotherm model shows that the dye removal isotherm for DR80 and DR23 can be approximated as Langmuir model. This means that the adsorption of DR80 and DR23 takes place at specific homogeneous sites.

3.5.5. Adsorption kinetics

The mechanism of pollutant adsorption onto an adsorbent can be investigated by determination of characteristic constants of adsorption using pseudo-first-order equation [56], pseudo-second-order equation [57], and intraparticle diffusion [58]. A linear form of pseudo-first-order model is:

$$\log\left(q_e - q_t\right) = \log\left(q_e\right) - \frac{k_1}{2.303}t \tag{15}$$

where q_e is the amount of dye adsorbed at equilibrium (mg g^{-1}), q_t is the amount of dye adsorbed at t time (mg g^{-1}) and k_1 is the equilibrium rate constant of pseudo-first-order adsorption (min^{-1}).

The pseudo-second-order adsorption model, in its final form, can be expressed as follows [59]:

$$\frac{t}{q_t} = \frac{1}{k_2 q_e^2} + \frac{1}{q_e}t \tag{16}$$

In Eq. (10) q_e is the amount of dye adsorbed at equilibrium (mg g^{-1}) and k_2 is the pseudo-second-order equilibrium rate constant (g mg^{-1} min).

As intra-particle diffusion resistance affects adsorption, it was explored by using the intraparticle diffusion model as:

$$q_t = k_p t^{1/2} + I \tag{17}$$

where k_p and I are the intra-particle diffusion rate constant and intercept, respectively.

Intra-particle diffusion is the rate controlling step when the lines of uptake pass through the origin. When the plots do not pass through the origin, some degree of boundary layer

Table 15
Linearized isotherm coefficients for dye adsorption at different dye concentration

Adsorbent	Langmuir			Freundlich			Tempkin		
	Q_0	K_L	R^2	$1/n$	K_F	R^2	K_T	B_1	R^2
DR80	3,333.33	0.600	0.999	0.167	1,584.89	0.856	48.81	388.54	0.880
DR23	2,500	0.307	0.998	0.182	1,202.26	0.923	15.98	364.07	0.930

control is involved, and it can be concluded the intra-particle diffusion is not only the rate limiting step.

In order to investigate the applicability of the pseudo-first-order, pseudo-second-order, and intra-particle diffusion models for the adsorption of DR80, and BR23 onto adsorbent at different dye concentration, linear plots of $\log(q_e - q_t)$ vs. contact time (t), t/q_t vs. contact time (t), and q_t against $t^{1/2}$, are plotted. The values of k_1, k_2, k_p, I, R^2 and the calculated q_e ($(q_e)_{Cal}$) are shown in Table 16.

The fact that the Langmuir isotherm fits the experimental data very well may be due to homogenous distribution of active sites on the PAMAM surface grafted PAN-DETA nanofiber surface; since the Langmuir equation assumes that the surface is homogenous. Although the R^2 values for adsorption of both dyes are bigger than 0.99, the fact that adsorption process was very fast and adsorption values were reasonably correlated by the Langmuir isotherm have also showed that the adsorption of both direct dyes occurs on the active sites onto nanofiber. Furthermore, *qe* values ($(q_e)_{Cal}$) calculated from the linear plots of t/q_t versus t for second-order kinetic model have showed a good agreement with experimental q_e values ($(q_e)_{Exp}$). As a result, it can be said that both direct dyes adsorption onto PAMAM surface grafted PAN-DETA nanofiber takes place according to the pseudo-second-order kinetic model.

3.6. Dye Removal Mechanisms by the PAMAM surface grafted PAN-DETA nanofiber

In general, the adsorption capacity depends on the chemical and physical properties of the surface of the adsorbent. Adsorption properties adsorbents toward ionic pollutants could be enhanced by introducing functional groups on their surface [60]. PAN is regarded as a good substrate for many applications due to the presence of nitrile groups in its structure which make it capable for easy chemical modification [61]. In this study, the PAN matrix was functionalized by DETA initially. After that, in order to increase the adsorption capacity of nanofibers toward anionic dyes, the surface of PAN-DETA composite nanofibers was modified by PAMAM. The higher adsorption capacity of surface grafted nanofibers may be explained to proceed via electrostatic interaction and hydrogen bond formation between the surface of the adsorbent and direct dye molecules. In the aqueous solution, the $-SO_3Na$ groups of the dye are converted to sulphonate groups ($-SO_3-$). Also, in the acidic pH, the amine groups of functionalized nanofiber become protonated. Then the electrostatic attraction could occur between the positively charged protonated amino grou=ps on the adsorbent surface and the negatively charged sulfonate of the dyes. Besides

Table 16
Kinetic constants for dye adsorption on PAMAM surface grafted PAN-DETA nanofibers at different dye concentration

Dye (mg L^{-1})	$(q_e)_{Exp}$	Pseudo-first-order			Pseudo-second-order			Intraparticle diffusion		
		R^2	$(q_e)_{Cal}$	k_1	R^2	$(q_e)_{Cal}$	k_2	R^2	I	k_p
DR80										
40	1,845	0.953	1,230	0.140	0.993	1,754.38	0.006	0.658	627.02	201.37
60	2,561.7	0.966	1,584.89	0.136	0.994	2,500	0.009	0.664	861.23	281
80	2,852	0.974	1,949.84	0.133	0.993	2,777.77	0.068	0.694	907.61	318.5
100	2,855	0.968	2,344.22	0.133	0.993	2,857.14	0.13	0.742	823.33	327.83
DR23										
40	1,662.2	0.964	1,148.15	0.131	0.994	1,428.57	0.006	0.704	516.5	187.65
60	2,103.6	0.968	1,621.81	0.128	0.992	2,065.26	0.007	0.744	599.95	243.09
80	2,380	0.963	2,000	0.130	0.993	2,294.56	0.010	0.803	576.51	285.94
100	2,360	0.969	2,000	0.129	0.993	2,478.56	0.011	0.841	490.66	293.54

Table 17
The maximum adsorption capacity of PAMAM grafted PAN-DETA nanofiber for DR80 and DR23 with other previously prepared adsorbents

Adsorbent	Adsorption capacity (mg g^{-1})	Dye	Ref.
PAN/DETA composite nanofiber	1,250	Direct red 80 (DR80)	35
PAN/PAMAM composite nanofiber	2,000	Direct red 80 (DR80)	22
	2,000	Direct red 23 (DR23)	
Iminated Polyacrylonitrile nanoparticle	54	Methylene blue (MB)	59
β-cyclodextrin/polyacrylonitrile Composite Nanofibers	90	methylene blue (MB)	62
hydrolyzed polyacrylonitrile fibres	49.5	reactive brilliant red HE-3B	63
PAMAM grafted PAN-DETA nanofiber	3,333.33	Direct red 80 (DR80)	Current study
	2,500	Direct red 23 (DR23)	

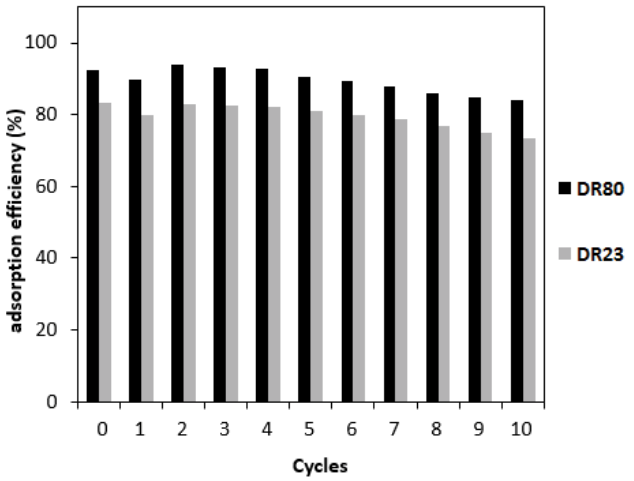

Fig. 12. The adsorption efficiency of nanofibers for DR80 and DR23 dyes at different regeneration cycles.

that, a great distinction of the direct dyes is the number of hydrophilic functional groups, which have a strong tendency to form hydrogen bonds with functionalized PAN nanofiber. In addition, dye molecules are encapsulated by the PAMAM dendrimer which causes to raise the dye removal efficiency [59,62,63].

A comparison between the synthesized nanofibers and previously synthesized adsorbents indicated on the higher adsorption capacity of PAMAM grafted PAN-DETA nanofibers (Table 17) [22,35,59,62,63].

3.7. Regeneration and reuse ability

The prepared nanofibers possess a large number of amine groups on their surface. In this regard, the regeneration process was performed in a NaOH solution. Fig. 12 shows the adsorption efficiency of nanofibers for DR80 and DR23 dyes at different cycles. It was clear that the removal percentage was gradually decreased in the consecutive cycles. It can be attributed to the irreversible deformation of nanofibers and the residual dyes in the voids of nanofiber assembly [61,64]. Also, the adsorption efficiency showed a sudden decrease in the first regeneration cycle which was due to the penetration of dyes into some adsorbent pores that full recovery is not possible. The similar result was stated by researchers [65]. However, the efficiency of the nanofibers was maintained high as 84.11% and 73.59% even after ten regeneration cycles for DR80 and DR23 dyes, respectively, indicating that the prepared nanofibers can be a good candidate for removing anionic dyes from solutions.

4. Conclusion

In this paper, PAMAM surface grafted PAN-DETA nanofiber was produced by electrospinning and its dye removal abilities were investigated. The surface modification process was performed by glutaraldehyde. ATR results confirmed successful grafting of PAMAM by the aid of glutaraldehyde. Imine groups are generated between PAMAM molecule and PAN-DETA webs by changes in the band intensities in the related spectra. SEM image showed the formation of a dense layer on the surface of nanofibers. Formation of the PAMAM layer on the surface and swelling of nanofiber raised the nanofiber diameter which caused to decrease the total surface area values and increase the average pore size values. Also, AFM results presented an increment in values of average roughness for PAN-DETA and PAMAM grafted PAN-DETA nanofibers compared to untreated PAN nanofiber. In order to investigate the dye removal ability, DR80 and DR23 were used as the model compound. Optimization of the process by RSM showed 95% dye removal efficiency under optimized operational conditions. The dye adsorption followed with Langmuir isotherm with the maximum adsorption capacity (Q_0) of 3,333.33 and 2,500 mg g^{-1} for DR80 and DR23, respectively. The adsorption kinetic of dyes was found to conform to the pseudo-second-order model, introducing our surface grafted PAN nanofibers as a novel fibrous adsorbent with high anionic dye adsorption capacity.

References

[1] Q. Qin, J. Ma, K. Liu, Adsorption of anionic dyes on ammonium-functionalized MCM-41, J. Hazard. Mater., 162 (2009) 133–139.
[2] C. Namasivayam, R. Radhika, S. Suba, Uptake of dyes by a promising locally available agricultural solid waste: coir pith, Waste Manage., 21 (2001) 381–387.
[3] N.M. Mahmoodi, Binary catalyst system dye degradation using photocatalysis, Fibers and Polymers 15(2014) 273–280.
[4] N.M. Mahmoodi, M. Arami, Numerical finite volume modeling of dye decolorization using immobilized titania nanophotocatalysis, Chem. Eng. J., 146 (2009) 189–193.
[5] N.M. Mahmoodi, M. Arami, N.Y. Limaee, K. Gharanjig, F. Nourmohammadian, Nanophotocatalysis using immobilized titanium dioxide nanoparticle: degradation and mineralization of water containing organic pollutant: case study of Butachlor, Mater. Res. Bull., 42 (2007) 797–806.
[6] N.M. Mahmoodi, N.Y. Limaee, M. Arami, S. Borhany, M. Mohammad-Taheri, Nanophotocatalysis using nanoparticles of titania: Mineralization and finite element modelling of Solophenyl dye decolorization, J. Photochem. Photobiol. A: Chem., 189 (2007) 1–6.
[7] S. Davarpanah, N.M. Mahmoodi, M. Arami, H. Bahrami, F. Mazaheri, Environmentally friendly surface modification of silk fiber: Chitosan grafting and dyeing, Appl. Surf. Sci., 255 (2009) 4171–4176.
[8] M. Ranjbar-Mohammadi, M. Arami, H. Bahrami, F. Mazaheri, N.M. Mahmoodi, Grafting of chitosan as a biopolymer onto wool fabric using anhydride bridge and its antibacterial property, Colloids and Surfaces B: Biointerfaces, 76 (2010) 397–403.
[9] N.M. Mahmoodi, M. Arabloo, J. Abdi, Laccase immobilized manganese ferrite nanoparticle: Synthesis and LSSVM intelligent modeling of decolorization, Water Res., 67 (2014) 216–226.
[10] M.S.M. Eldin, S.A. El-Sakka, M.M. El-Masry, I.I. Abdel-Gawad, S.S. Garybe, Removal of methylene blue dye from aqueous medium by nano poly acrylonitrile particles, Desal. Wat. Treat., 44 (2012) 151–160.
[11] Y. Bao, X. Yan, W. Du, X. Xie, Z. Pan, J. Zhou, L. Li, Application of amine-functionalized MCM-41 modified ultrafiltration membrane to remove chromium (VI) and copper (II), Chem. Eng. J., 281 (2015) 460–467.
[12] M. SliwkaKaszyńska, K. Jaszczołt, A. Kołodziejczyk, J. Rachoń, 1,3-Alternate 25,27-dibenzoiloxy-26,28-bis-[3-propyloxy]-calix[4] arene-bonded silica gel as a new type of HPLC stationary phase, Talanta, 68 (2006) 1560–1566.
[13] A.R. Cestari, E.F. Vieira, G.S. Vieira, L.E. Almeida, The removal of anionic dyes from aqueous solutions in the presence of

anionic surfactant using aminopropylsilica—A kinetic study, J. Hazard. Mater., 138 (2006) 133–141.
[14] J. Lin, J.A. Siddiqui, R.M. Ottenbrite, Surface modification of inorganic oxide particles with silane coupling agent and organic dyes, Polym. Adv. Technol., 12 (2001) 285–292.
[15] N.M. Mahmoodi, Synthesis of core–shell magnetic adsorbent nanoparticle and selectivity analysis for binary system dye removal, J. Ind. Eng. Chem., 20 (2014) 2050–2058.
[16] Y. Yan, Q. An, Z. Xiao, W. Zheng, S. Zhai, Flexible core-shell/bead-like alginate@PEI with exceptional adsorption capacity, recycling performance toward batch and column sorption of Cr(VI), Chem. Eng. J., 313 (2017) 475–486.
[17] D. Bilba, D. Suteu, T. Malutan, Removal of reactive dye brilliant red HE-3B from aqueous solutions by hydrolyzed polyacrylonitrile fibres: equilibrium and kinetics modelling, Open Chem., 6 (2008) 258–266.
[18] N.M. Mahmoodi, Synthesis of amine-functionalized magnetic ferrite nanoparticle and its dye removal ability, J. Environ. Eng., 139 (2013) 1382–1390.
[19] S. Deng, R. Bai, J.P. Chen, Behaviors and mechanisms of copper adsorption on hydrolyzed polyacrylonitrile fibers, J. Colloid Interface Sci., 260 (2003) 265–272.
[20] A. Almasian, M.E. Olya, N.M. Mahmoodi, Synthesis of polyacrylonitrile/polyamidoamine composite nanofibers using electrospinning technique and their dye removal capacity, J. Taiwan Inst. Chem. Eng., 49 (2015) 119–128.
[21] V.K. Yellepeddi, A. Kumar, S. Palakurthi, Surface modified poly(amido)amine dendrimers as diverse nanomolecules for biomedical applications, Expert Opin. Drug Deliv., 6 (2009) 835–850.
[22] D. Astruc, E. Boisselier, C. Ornelas, Dendrimers designed for functions: from physical, photophysical, and supramolecular properties to applications in sensing, catalysis, molecular electronics, photonics, and nanomedicine, Chem. Rev., 110 (2010) 1857–1959.
[23] L. Lianchao, W. Baoguo, T. Huimin, C. Tianlu, X. Jiping, A novel nanofiltration membrane prepared with PAMAM and TMC by in situ interfacial polymerization on PEK-C ultrafiltration membrane, J. Membr. Sci., 269 (2006) 84–93.
[24] N. Pérignon, J.D. Marty, A.F. Mingotaud, M. Dumont, I. Rico-Lattes, C. Mingotaud, Hyperbranched polymers analogous to PAMAM dendrimers for the formation and stabilization of gold nanoparticles, Macromolecules, 40 (2007) 3034–3041.
[25] S. Deng, R. Bai, Removal of trivalent and hexavalent chromium with aminated polyacrylonitrile fibers: performance and mechanisms, Water Res., 38 (2004) 2424–2432.
[26] D.H. Shin, Y.G. Ko, U.S. Choi, W.N. Kim, Design of high efficiency chelate fibers with an amine group to remove heavy metal ions and pH-related FT-IR analysis, Ind. Eng. Chem. Res., 43 (2004) 2060–2066.
[27] P.K. Neghlani, M. Rafizadeh, F.A. Taromi, Preparation of aminated-polyacrylonitrile nanofiber membranes for the adsorption of metal ions: comparison with microfibers, J. Hazard. Mater., 186 (2011) 182–189.
[28] H. Yoo, S.-Y. Kwak, Surface functionalization of PTFE membranes with hyperbranched poly(amidoamine) for the removal of Cu^{2+} ions from aqueous solution, J. Membr. Sci., 448 (2013) 125–134.
[29] K.N. Han, B.Y. Yu, S.-Y. Kwak, Hyperbranched poly (amidoamine)/polysulfone composite membranes for Cd(II) removal from water, J. Membr. Sci., 396 (2012) 83–91.
[30] G.C. Fard, M. Mirjalili, A. Almasian, F. Najafi, PAMAM grafted α-Fe_2O_3 nanofiber: Preparation and dye removal ability from binary system, J. Taiwan Inst. Chem. Eng., 80 (2017) 156–167.
[31] N.M. Mahmoodi, Dendrimer functionalized nanoarchitecture: Synthesis and binary system dye removal, J. Taiwan Inst. Chem. Eng., 45 (2014) 2008–2020.
[32] H.J. Kumari, P. Krishnamoorthy, T.K. Arumugam, S. Radhakrishnan, D. Vasudevan, An efficient removal of crystal violet dye from waste water by adsorption onto TLAC/chitosan composite: a novel low cost adsorbent, Int. J. Biol. Macromol., 96 (2017) 324–333.
[33] G.C. Fard, M. Mirjalili, F. Najafi, Hydroxylated α-Fe_2O_3 nanofiber: Optimization of synthesis conditions, anionic dyes adsorption kinetic, isotherm and error analysis, J. Taiwan Inst. Chem. Eng., 70 (2017) 188–199.
[34] G.L. Dotto, J.M.N. Santos, E.H. Tanabe, D.A. Bertuol, E.L. Foletto, E.C. Lima, F.A. Pavan, Chitosan/polyamide nanofibers prepared by Forcespinning® technology: a new adsorbent to remove anionic dyes from aqueous solutions, J. Cleaner Prod., 144 (2017) 120–129.
[35] A. Almasian, M.E. Olya, N.M. Mahmoodi, Preparation and adsorption behavior of diethylenetriamine/polyacrylonitrile composite nanofibers for a direct dye removal, Fibers Polym., 16 (2015) 1925–1934.
[36] R.H. Myers, D.C. Montgomery, G.G. Vining, T.J. Robinson, Generalized Linear Models: With Applications in Engineering and the Sciences, John Wiley & Sons, Inc., Hoboken, New Jersey, USA, 2012.
[37] W.H. Woodall, D.C. Montgomery, Research issues and ideas in statistical process control, J. Qual. Technol., 31 (1999) 376–386.
[38] R.H. Myers, Response Surface Methodology, Allyn & Bacon, Boston, USA, 1971.
[39] Y.J. Ryu, H.Y. Kim, K.H. Lee, H.C. Park, D.R. Lee, Transport properties of electrospun nylon 6 nonwoven mats, Eur. Polym. J., 39 (2003) 1883–1889.
[40] N.M. Mahmoodi, Synthesis of core–shell magnetic adsorbent nanoparticle and selectivity analysis for binary system dye removal, J. Ind. Eng. Chem., 20 (2014) 2050–2058.
[41] S. Sadekar, H. Ghandehari, Transepithelial transport and toxicity of PAMAM dendrimers: Implications for oral drug delivery, Adv. Drug Delivery Rev., 64 (2012) 571–588.
[42] M.N.R. Kumar, A review of chitin and chitosan applications, React. Funct. Polym., 46 (2000) 1–27.
[43] K. Suttiponparnit, J. Jiang, M. Sahu, S. Suvachittanont, T. Charinpanitkul, P. Biswas, Role of surface area, primary particle size, and crystal phase on titanium dioxide nanoparticle dispersion properties, Nanoscale Res. Lett., 6 (2010) 27.
[44] M. Müller, J. Meier-Haack, S. Schwarz, H.M. Buchhammer, K.J. Eichhorn, A. Janke, B. Keßler, J. Nagel, M. Oelmann, T. Reihs, K. Lunkwitz, Polyelectrolyte multilayers and their interactions, J. Adhes., 80 (2004) 521–547.
[45] N.M. Mahmoodi, Nickel ferrite nanoparticle: synthesis, modification by surfactant and dye removal ability, Water Air Soil Pollut., 224 (2013) 1419.
[46] G. Crini, P.-M. Badot, Application of chitosan, a natural aminopolysaccharide, for dye removal from aqueous solutions by adsorption processes using batch studies: a review of recent literature, Program Polym. Sci., 33 (2008) 399–447.
[47] M.S. Chiou, H.Y.Li, Adsorption behaviour of reactive dye in aqueous solution on chemical cross-linked chitosan beads, Chemosphere, 50 (2003) 1095–1105.
[48] C. Ng, J.N. Losso, W.E. Marshall, R.M. Rao, Freundlich adsorption isotherms of agricultural by-product-based powdered activated carbons in a geosmin-water system, Bioresour. Technol., 85 (2002) 131–135.
[49] I. Langmuir, The adsorption of gases on plane surfaces of glass, mica and platinum, J. Am. Chem. Soc., 40 (1918) 1361–1403.
[50] M.E. Argun, S. Dursun, M. Karatas, M. Gürü, Activation of pine cone using Fenton oxidation for Cd(II) and Pb(II) removal, Bioresour. Technol., 99 (2008) 8691–8698.
[51] F. Woodard, Industrial Waste Treatment Handbook, Woodard & Curran, Inc., Portland, Maine, USA, 2001.
[52] L.D. Benefield, J.F. Judkins, B.L. Weand, Process Chemistry for Water and Wastewater Treatment, Prentice-Hall, Englewood Cliffs, New Jersey, USA, 1982.
[53] K.K. Choy, J.F. Porter, G. Mckay, Intraparticle diffusion in single and multicomponent acid dye adsorption from wastewater onto carbon, Chem. Eng. J., 103 (2004) 133–145.
[54] M.J. Temkin, V. Pyzhev, Recent modifications to Langmuir isotherms, Acta Phys. Chim. Sin., 12 (1940) 217–222.

[55] S. Lagergren, About the theory of so-called adsorption of soluble substances, Kungliga Svenska Vetenskapsakademiens Handlingar, 24 (1898) 1–39.
[56] B. Hayati, N.M. Mahmoodi. Modification of activated carbon by alkaline to remove dyes from wastewater: mechanism, isotherm and kinetic, Desalin. Water Treat., 47 (2012) 322–333.
[57] W.J. Weber, J.C. Morris, Kinetics of adsorption on carbon from solution, J. Sanit. Eng. Div., 89 (1963) 31–60.
[58] M. Monier, D.M. Ayad, A.A. Sarhan, Adsorption of Cu(II), Hg(II), and Ni(II) ions by modified natural wool chelating fibers, J. Hazard. Mater., 176 (2010) 348–355.
[59] M.S. Diallo, W. Arasho, J.H. Johnson, W.A. Goddard 3rd, Dendritic chelating agents. 2. U(VI) binding to poly(amidoamine) and poly(propyleneimine) dendrimers in aqueous solutions, Environ. Sci. Technol., 42 (2008) 1572–1579.
[60] D. Chauhan, J. Dwivedi, N. Sankararamakrishnan, Facile synthesis of smart biopolymeric nanofibers towards toxic ion removal and disinfection control, RSC Adv., 4 (2014) 54694–54702.
[61] A. Almasian, M.L. Jalali, G.C. Fard, L. Maleknia, Surfactant grafted PDA-PAN nanofiber: optimization of synthesis, characterization and oil absorption property, Chem. Eng. J., 326 (2017) 1232–1241.
[62] A. Asthana, N.K. Jain, Dendrimers: novel polymeric nano-architectures for solubility enhancement, Biomacromolecules, 7 (2006) 649–658.
[63] C. Yiyun, Y. Jiepin, Effect of polyamidoamine dendrimers in decolorising triarylmethane dye effluent, Color Technol., 121 (2005) 72–75.
[64] J. Wu, N. Wang, L. Wang, H. Dong, Y. Zhao, L. Jiang, Electrospunporous structure fibrous film with high oil adsorption capacity, ACS Appl. Mater. Interfaces, 4 (2012) 3207–3212.
[65] J. Wang, Y. Zheng, A. Wang, Superhydrophobic kapok fiber oil-absorbent: preparation and high oil absorbency, Chem. Eng. J., 213 (2012) 1–7.